AD-A133 467 VORTEX SHEDDING AND LASER ABLATION(U) NAVAL RESEARCH 1/1
LAB WASHINGTON DC M H EMERY ET AL. 22 SEP 83
NRL-MR-5089

UNCLASSIFIED F/G 20/4 NL

END
DATE FILMED
DTIC

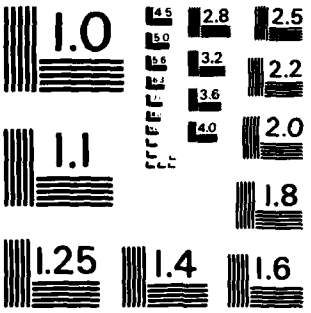

MICROCOPY RESOLUTION TEST CHART
NATIONAL BUREAU OF STANDARDS - 1963 - A

SECURITY CLASSIFICATION OF THIS PAGE (When Data Entered)

REPORT DOCUMENTATION PAGE	READ INSTRUCTIONS BEFORE COMPLETING FORM
1. REPORT NUMBER: NRL Memorandum Report 5089 — 2. GOVT ACCESSION NO.: AD-A133 47	3. RECIPIENT'S CATALOG NUMBER:
4. TITLE (and Subtitle): VORTEX SHEDDING AND LASER ABLATION	5. TYPE OF REPORT & PERIOD COVERED: Interim report on a continuing NRL problem.
	6. PERFORMING ORG. REPORT NUMBER:
7. AUTHOR(s): M.H. Emery, J.H. Gardner, J.P. Boris, and A.L. Cooper	8. CONTRACT OR GRANT NUMBER(s):
9. PERFORMING ORGANIZATION NAME AND ADDRESS: Naval Research Laboratory, Washington, DC 20375	10. PROGRAM ELEMENT, PROJECT, TASK AREA & WORK UNIT NUMBERS: 44-0859-A-3
11. CONTROLLING OFFICE NAME AND ADDRESS:	12. REPORT DATE: September 22, 1983
	13. NUMBER OF PAGES: 13
14. MONITORING AGENCY NAME & ADDRESS (if different from Controlling Office):	15. SECURITY CLASS. (of this report): UNCLASSIFIED
	15a. DECLASSIFICATION/DOWNGRADING SCHEDULE:

16. DISTRIBUTION STATEMENT (of this Report)

Approved for public release; distribution unlimited.

17. DISTRIBUTION STATEMENT (of the abstract entered in Block 20, if different from Report)

18. SUPPLEMENTARY NOTES

This work was supported by the U.S. Department of Energy and the Office of Naval Research.

19. KEY WORDS (Continue on reverse side if necessary and identify by block number)

Rayleigh-Taylor
Vortex shedding
Laser ablation
Magnetic fields
Flux inhibition
Hydrodynamics
Numerical simulation

20. ABSTRACT (Continue on reverse side if necessary and identify by block number)

Through a critical examination of the vortex dynamics of laser ablatively accelerated targets we are able to explain the inhibited linear Rayleigh-Taylor growth rates, clarify the role of the Kelvin-Helmholtz roll-up, explain the short wavelength cutoff, explain and theoretically reproduce dynamically stabilized growth rates and predict magnetic field structures throughout the overdense region which lead to a physically motivated model of thermal flux inhibition.

DD FORM 1 JAN 73 1473 EDITION OF 1 NOV 65 IS OBSOLETE
S/N 0102-014-6601

SECURITY CLASSIFICATION OF THIS PAGE (When Data Entered)

VORTEX SHEDDING AND LASER ABLATION

The Rayleigh-Taylor[1] (RT) instability is a potential obstacle to inertial confinement fusion in that it can destroy the symmetry of the imploding shell. The RT instability can occur anywhere in the shell when the profiles become baroclinic, i.e., possess, non-collinear density and pressure gradients. The ablation layer, which separates the cold, high-density shell from the hot, low-density ablating plasma, is particularly susceptible to RT growth. Several researchers[2,3], including ourselves[4,5], have reported the results of numerical simultions of the RT instability in laser ablatively accelerated targets. The results were consistent only in that the linear growth rates were below the classically predicted values ($\gamma_c = (kg)^{1/2}$). Several mechanisms have been proposed to explain the reduced linear growth of the instability including thin layer effects[6], finite density gradients[6], mass ablative effects[2], fire-polishing[7], mass transfer[8], finite thermal conduction[8] and compressibility[9] effects.

In Fig. 1 we compare the results of the thin layer model[6], the exponential density gradient model[6] and a modified version (the latent heat is the entropy change across the ablation layer) of the boiling film model[8] to the classical and numerically obtained results. The boiling film model includes mass and thermal transfer across the interface. The numerical results were obtained with our two-dimensional Cartesian simulation code FAST2D[4,5] using a sliding, varibly-spaced, Eulerian grid. The simulations were done for a 20 μm thick, plastic (CH) foil irradiated with a 1.06 μm laser with an absorbed intensity of 10^{13} W/cm^2. The initial steady-state density profile had its density peak perturbed with a single sinusoidal mode corresponding to a total mass perturbation of 1%. The number of e-foldings was 8.0 ± 0.4 for

Manuscript approved June 2, 1983.

all the modes investigated. It is apparent that the classical solution is the only one that yields the same k-dependence as the numerical results, albeit with a growth rate larger than the numerical value.

Recently it has been shown that compressibility is a destabilizing mechanism[10] and mass ablation, or tip erosion[2], is viable for stabilization only if the mass ablation rate ($\dot{m}_{ab}$) is greater than the rate of mass flow into the spike ($\dot{m}_{rt}$). We now show that this is true only for extremely short wavelength laser light. $\dot{m}_{ab}$ (gm $cm^{-1}s^{-1}$) = $\rho v L = \rho_c v_c L$ where the subscript c denotes the density (ρ) and velocity (v) at the critical surface and L is some length along the ablation surface. $\dot{m}_{rt} = \rho v_s L$ where v_s is the velocity of fall of the spike. In the linear regime, the amplitude of the spike is $a = a_o \cosh((kg)^{1/2}t)$; thus for short times, say one e-folding, $v_s \approx 0.3(\lambda_{rt} g)^{1/2}$ (for $a_o = 0.1\lambda_{rt}$, $\lambda_{rt} = 2\pi/k$, the perturbation wavelength). Now $g = P_a/M$ where P_a is the ablation pressure (dynes-cm^{-2}) and $M = \rho a$ is the mass (gm-cm^{-2}) of the spike of amplitude a. In the linear regime $a < 1/2\lambda_{rt}$ and for short times $a \approx 0.15\lambda_{rt}$. From steady state planar ablative flow models[11] we have $v_c = 9.3 \times 10^2 (I\lambda^2)^{1/3}$ cm/sec and $P_a = 5.6 \times 10^3 (I/\lambda)^{2/3}$ dynes/cm^2, where I is the absorbed irradiance (W/cm^2) and λ is the laser wavelength (μm). This gives a condition on laser wavelength for mass ablation to dominate RT growth that $\lambda(\mu m) \leq 3.0 \times 10^{-2} A/(Z+1)\rho^{-1/2}$, where A is the atomic number, Z is the charge state and ρ is the density of the slab (gm-cm^{-3}). Note that for this model the laser intensity and perturbation wavelength scale out of the problem. When the spike amplitude is about half the perturbation wavelength the spike goes into freefall[5]. Under those conditions the spike velocity can be written as $v_s \approx (2P_a/\rho)^{1/2}$ and $\lambda \lesssim 1.6 \times 10^{-2} A/(Z+1)\rho^{-1/2}$; thus, a more stringent condition applies in the nonlinear regime. Since the above models have

failed to adequately explain the reduced linear RT growth and the $k^{1/2}$ dependence we propose here a new ablative-like inhibition mechanism - the ablation of vorticity.

In the case of a finite-sized density gradient, the discontinuous vortex sheet of the classical RT problem is replaced by a finite-thickness vortex layer. The rate of change of the vorticity ($\vec{\omega} = \omega \vec{e}_z = \nabla \times \vec{u}(x,y)$) following a fluid element is given by $d\vec{\omega}/dt = \partial\vec{\omega}/\partial t + \vec{u}\cdot\nabla\vec{\omega} = \nabla\rho \times \nabla p/\rho^2 - \vec{\omega}\nabla\cdot\vec{u}$ where ρ is the mass density and p is the pressure. The second term on the right-hand side is the compressibility term and is typically quite small in our simulations. The first term on the RHS is the baroclinic vector and is the source term for the vorticity. Fig. 2a shows the contours of constant $d\vec{\omega}/dt$ for a 20 μm wavelength 1% density perturbation.

The vorticity that arises from the differential twisting of the density and pressure surfaces feeds the "heavy" material into the spike and the "light" material into the bubble. Part of the vorticity generated in the unstable layer is ablated and periodically shed into the blowoff thus reducing the linear RT growth. Figure 2b illustrates this shedding when the RT instability is in the linear regime (3.97 ns). The portion of the foil which is convex towards the laser (the spike) is now shedding vorticity into the blowoff. As the magnitude of this vorticity increases it draws fluid of opposite vorticity across the wake cutting off the growing vortex from a further supply of circulation. The vortex then separates from the ablation layer and is convected downstream into the blowoff. The interaction of vortices of opposite sign results in a relatively constant periodic shedding from both the convex (spike) and concave (bubble) portions of the foil while

the system is in the linear regime. This vortex shedding process is very similar to the flow about a bluff body[12] characterized by the universal Strouhal number[13] a dimensionless shedding frequency. (The baroclinic term plays the role of the bluff body viscous boundary layer). $S = \frac{fd_w}{u_w}$, where f is the shedding frequency, d_w is the width of the wake and u_w is the velocity at separation. S = 0.18 and is constant for a wide range of Reynolds numbers and body shapes. We compare the measured (between successive sheddings from the spike) and calculated ($f = 0.18\ u_w/d_w$) shedding frequency as a function of perturbation wavelength in Fig. 3. To within a constant factor, the agreement is quite good for the longer wavelength modes. The anomalous increase in the measured shedding rate for the short wavelength modes is similar to the rapid increase in Strouhal frequency when pairs of cylinders are close together.[14]

To account for the reduced linear RT growth as a result of this vortex shedding process we write the RT growth rate as $\gamma_{vs} = (kg)^{1/2} - \alpha f$, where α is some fraction of the measured shedding frequency. We set $\alpha = 0.4$ to fit the 20 μm mode. Figure 1 shows good agreement between the computational growth rates and the rates obtained from the vortex shedding theory (X). An $\alpha = 0.4$ corresponds to a defect ratio of 0.4; i.e. a measured loss of vorticity due to vortex merging at the ablation layer of approximately 60% and is in agreement with the analogous flow past a bluff body[12].

As the spike grows in amplitude it begins to shield the bubble from the ablation process. As a result, the vorticity is advected down the sides of

the spikes until the temperature gradient is sufficiently large to cause ablation (Fig. 2c). The linear RT growth begins to saturate when the amplitude of the spike is equal to approximately half the wavelength of the perturbation. The sides of the spikes cease ablating and the vorticies begin collecting behind the heads of the spike causing the KH roll-up of the spike tips proportional to the wavenumber reported previously[4,5] (Fig. 2d).

It is well known[14] that when the separation between pairs of cylinders is less than twice the diameter of the cylinder the Strouhal frequency increases well above that for a single cylinder by a factor of ~ 5/3. We find a similar increase in the shedding frequencies for the short wavelength cases. This leads to a scaling law that relates the separation of the vortices ($\lambda_{rt}/2$) to their area and predicts an increase in the Strouhal frequency, thus enforcing the short wavelength cutoff of the RT mode, for $\lambda_{rt} < 8b$ where b is the thickness of the shear layer at the ablation front. b scales as $I^{-1/3}$ and is independent of the foil thickness. Figure 4 compares the predicted short wavelength cutoff value (vertical arrows) to the FAST2D simulation results. Also see Fig. 1.

Vortex dynamics may also be used to explain the results of dynamic stabilization of long wavelength modes reported several years ago[15]. It is also well known that if a bluff body is oscillated in line with or transverse to a uniform flow with a frequency near the Strouhal shedding frequency, the vortices will shed at the impressed frequency[13]. In the ablation case the equivalent effect[15] was achieved by oscillating the laser intensity by 25% at a frequency of $3\times10^9 s^{-1}$. This would give a theoretical growth rate of $\gamma_{ds} = (kg)^{1/2} - .4f_{ds} = 3.0\times10^8 s^{-1}((kg)^{1/2} = 1.5\times10^9\ s^{-1})$, considerably

reduced below the unstabilized computational growth rate for the 100 μm mode of $\gamma_c = 9.8 \times 10^8\ s^{-1}$, in agreement with the computational results.

Another important consequence of the vortex dynamics is that it permits an analogy with the magnetic field structure. The baroclinic source term also contributes to the growth of a dc magnetic field[16] and, assuming the compressibility term is small, we find $\vec{B}(\text{Gauss}) = -1.04 \times 10^{-4} \frac{A}{(Z+1)} \vec{\omega}$, where A is the atomic number, Z the charge state and ω the vorticity (s^{-1}). Using this analogy we find typical field strengths at the ablation layer for all the RT modes investigated of 20-30 kG in the linear regime (after about 2 e-foldings) and 3-4 MG at the saturation level of the RT instability. The magnetic field saturates at the same time as the RT growth. These are toroidal magnetic fields and as a result of the ablation process and the fact that the magnetic Reynold's number $R_m > 1$ they fill the overdense region. Magnetic field generation due to the RT instability has also been simulated with a magnetohydrodynamic particle code[17], however, the profiles and initial conditions in that model were not characteristic of the typical laser-ablative experiments.

Magnetic fields will be generated at the ablation layer whenever the density and pressure profiles become non-collinear; i.e., by the RT instability, laser asymmetries and/or target imperfections, which may explain thermal flux inhibition. For a series of 2:1 laser asymmetry runs for various intensities we find that B falls off as r^{-1} away from the ablation layer and reaches a constant average value of $\langle B \rangle \sim 10\text{-}15$ kG out to the critical surface with a resistive decay time 3 times longer than the 3.5 ns pulse.

By comparing the thermal flux across a magnetic field $(q_\perp)$[18] to the uninhibited free-streaming flux (q_{fs}) it is easy to show $q_\perp = 5/Z(r_e/\lambda_{mfp})(r_e/L)q_{fs}$, where r_e is the electron gyroradius, λ_{mfp} is the electron mean free path and L is the thermal gradient scale length. From the asymmetry runs B = 15 kG at critical and for $I \leq 6\times10^{13}$ W/cm^2 for λ = 1.06 μm and $I < 10^{14}$ W/cm^2 for λ = 0.53 μm, $r_e/\lambda_{mfp} > 1$ and classical thermal flux applies. However, for $I = 1\times10^{14}$ W/cm^2 for λ = 1.06 μm, $r_e/\lambda_{mfp} = 0.7$ and L ≈ 700 μm, thus $q_\perp = .06\ q_{fs}$ giving rise to a moderate flux inhibition at this intensity. Assuming the same B = 15 kG and scaling $T_e \propto I^{2/5}$ and $L \propto I^{2/5}$, then we would predict a flux inhibition of 0.01 for 1.06 μm laser light at 10^{15} W/cm^2. This flux inhibition factor is somewhat smaller than those proposed to explain experimental results. This is most likely due to our overestimate of the magnetic field at critical since we have dropped the compressibility term. However, the flux inhibition from the magnetic field structure scales properly with laser intensity and wavelength.

In conclusion, we have shown that the vortex dynamics of laser ablation explains the inhibited RT growth, the KH rollup, the short-wavelength cutoff, dynamic stabilization and provides a possible mechanism for thermal flux inhibition resulting from magnetic fields in the overdense region.

Acknowledgements

The authors gratefully acknowledge the many stimulating conversations with S. Bodner and R. Whitlock at the Naval Research Laboratory. This work was supported by the U.S. Department of Energy and the Office of Naval Research.

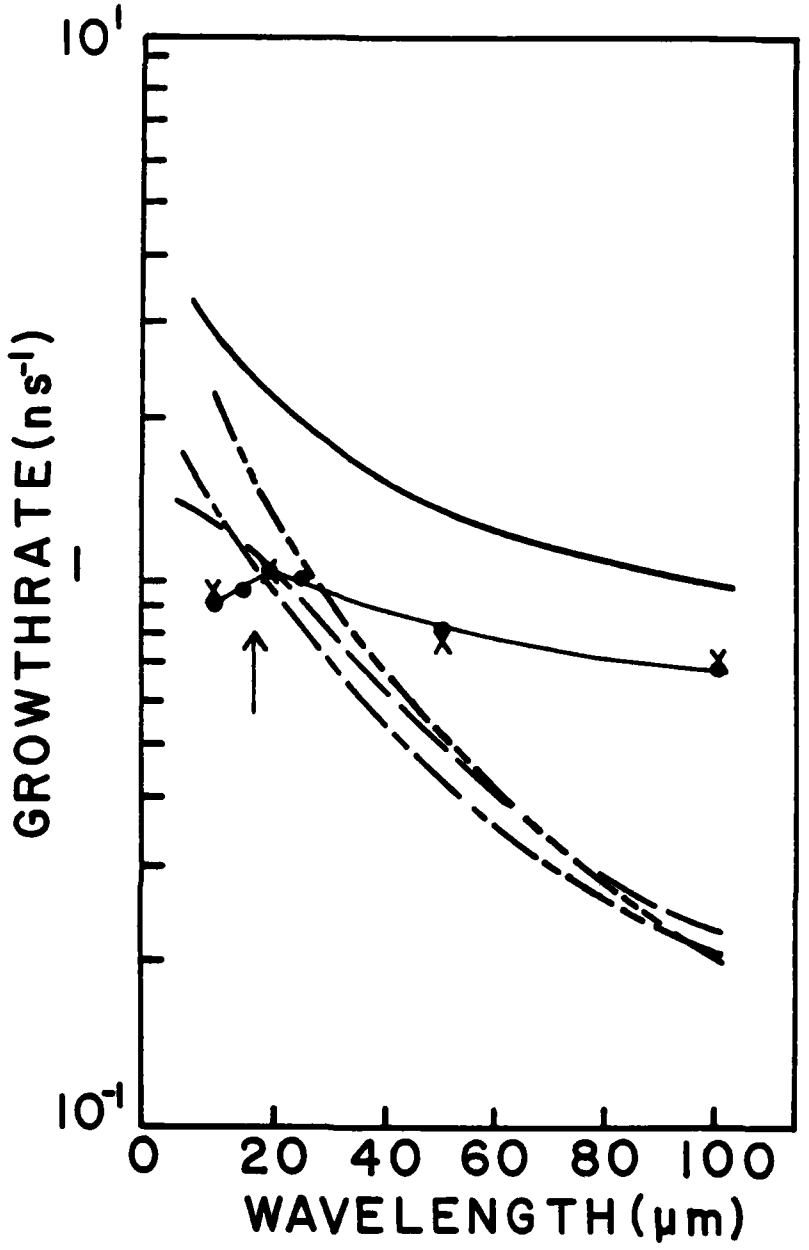

Figure 1

Comparison of the computational linear growth rate (—●—) to the classical solution (γ_c, ——) the thin layer solution (γ_{th}, ---) the exponential gradient solution γ_{ex}, —— – ——) and the mass and thermal transfer solution (γ_{mt}, —— – – ——). The X's are the theoretially predicted growth rates and the arrow indicates the predicted short wavelength cutoff.

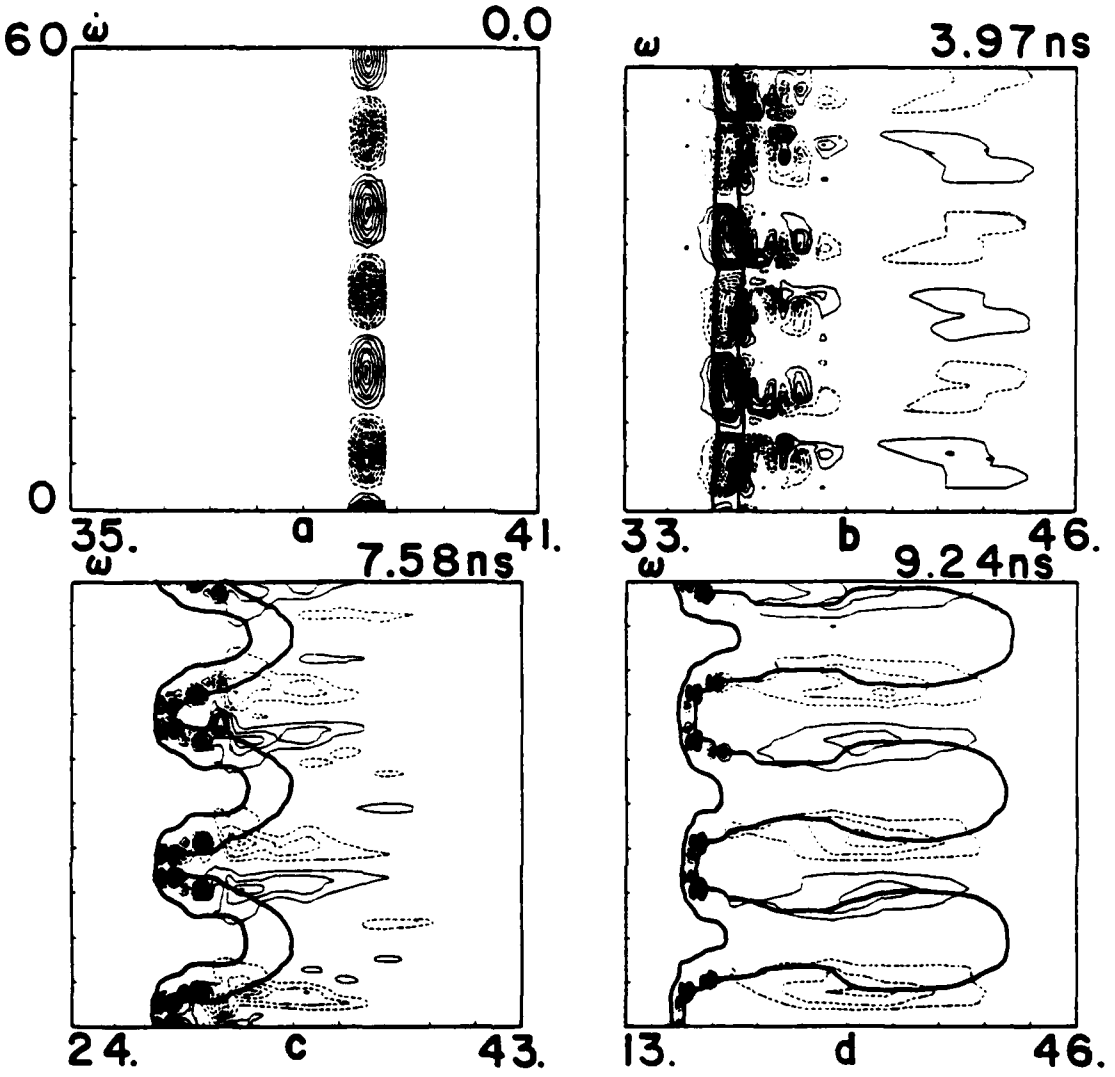

Figure 2

(a) Contours of constant baroclinicity ($d\vec{\omega}/dt$) (in 10% increments of the maximum ($\pm 3.2\times10^{16}s^{-2}$)) for a density perturbation with a wavelength of 20 μm. The solid (dashed) contours are for $d\vec{\omega}/dt >$ 0(<0). The centers of the contours are along the density peak. The laser is impinging the foil from the right. (b,c,d) Contours of constant vorticity, in 10% increments of the maximum ((b), $\pm 2.8\times10^{8}s^{-1}$; (c), $\pm 1.2\times10^{10}s^{-1}$; (d), $\pm 4.3\times10^{10}s^{-1}$), at various stages of the RT instability. The dashed (solid) contours indicate clockwise (counter-clockwise) rotation. The bold lines delineate the 10% (right) and 80% (left) density contours.

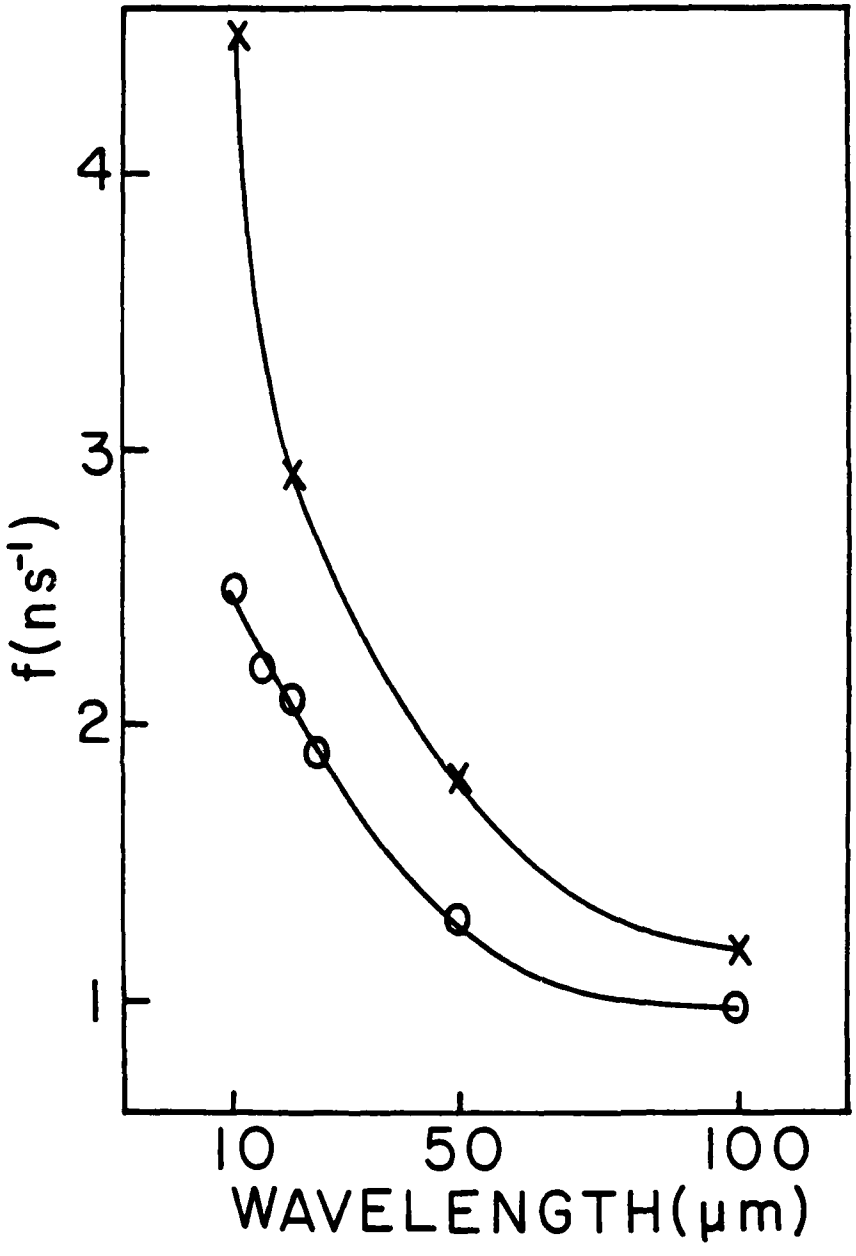

Figure 3

Comparison of the measured shedding frequency (x) to the value calculated with a constant universal Strouhal frequency of 0.18 (0).

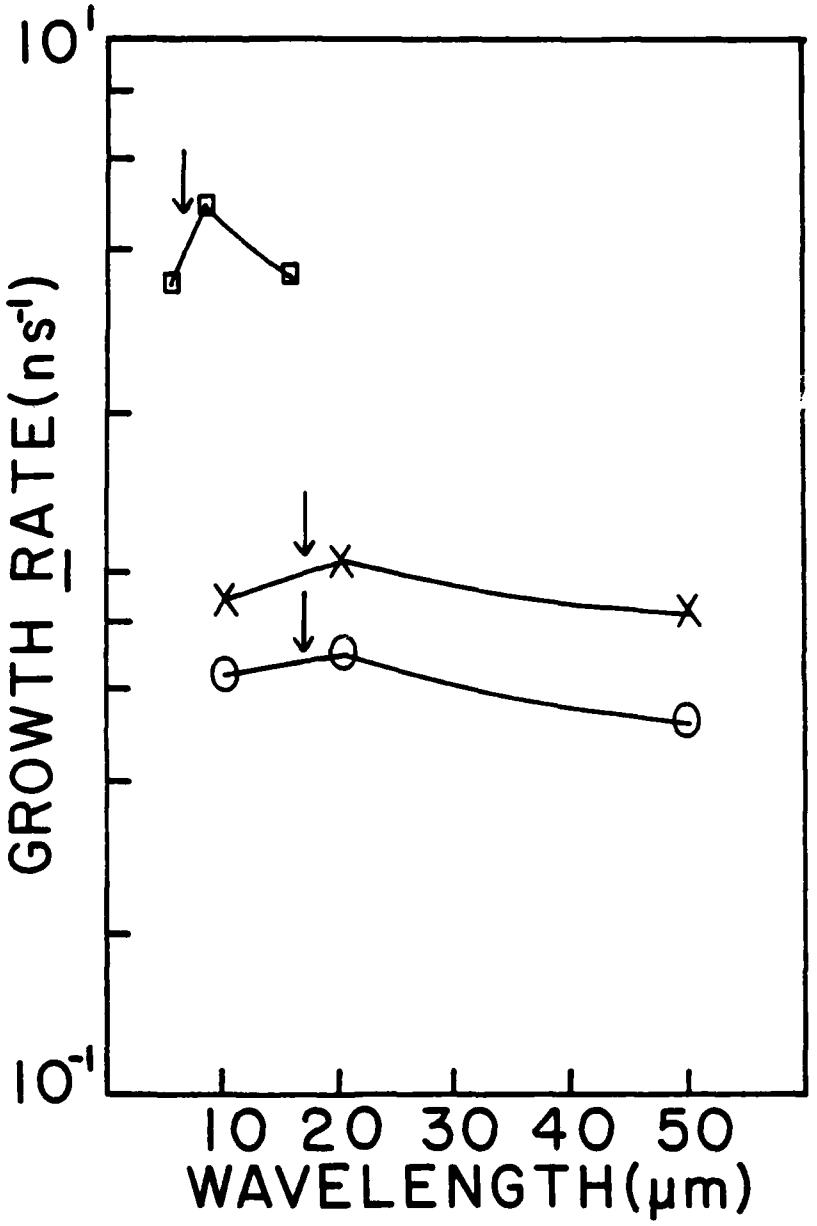

Figure 4

Comparison of the predicted short wavelength cutoff value (vertical arrow) to the simulation results for 7μm C, 10^{13} W/cm^2 (0), 8 μm CH, 10^{13} W/cm^2 (x) and 7μm C, 10^{14} W/cm^2 (□).

References

1. Lord Rayleigh, Theory of Sound (Dover, New York, 1945), 2nd ed., Vol. 2; G. Taylor, Proc. R. Soc. (London), Ser. A 201, 192 (1950).
2. R.L. McCrory, et al., Phys. Rev. Lett. 46, 336 (1981).
3. J.D. Lindl and W. C. Mead, Phys. Rev. Lett. 34, 1273 (1975).
4. M.H. Emery, et al., Phys. Rev. Lett. 48, 677 (1982).
5. M.H. Emery, et al., Appl. Phys. Lett. 41, 808 (1982).
6. H. Lamb, Hydrodynamics (Dover, New York, 1945), 6th ed.
7. S.E. Bodner, Phys. Rev. Lett. 33, 761 (1974).
8. D.Y. Hsieh, Trans. ASME 94D, 156 (1972).
9. P.O. Vandervoort, Astrophys. J. 134, 609 (1961).
10. D. Book and I. Bernstein, to be publ., Phys. Fluids.
11. W. M. Manheimer, et al., Phys. Fluids 25, 1644 (1982).
12. E. Berger and R. Wille, Ann. Rev. Fluid Mech. 4, 313 (1972).
13. O.M. Griffin, J. Fluid Mech. 85, 591 (1978); J. Fluids Eng. 103, 52 (1981).
14. M.M. Zdravkovich, Trans. ASME 99I, 618 (1977).
15. J.P. Boris, Comments Plasma Phys. Controlled Fusion 3, 1 (1977).
16. J.A. Stamper, et al., Phys. Rev. Lett. 26, 1012 (1971).
17. K. Mims, et al., Phys. Rev. Lett. 41, 1715 (1978).
18. S.I. Braginskii, Rev. Plasma Physics, Vol. 1 p. 205, (Consultants Bureau, New York, 1965).